Applied Nanoscience (2023) 13:3721–3733
https://doi.org/10.1007/s13204-022-02516-4

ORIGINAL ARTICLE

Studies on adsorption behavior of electrospun nanofibers for pollutant remediation from simulated wastewater

Dan Bahadur Pal[1] · Arvind Singh[3] · Roli Saini[2] · Neha Srivastava[2] · Khursheed Muzammil[4] · Irfan Ahmad[5] · Vijai Kumar Gupta[6,7]

Received: 15 January 2022 / Accepted: 21 May 2022 / Published online: 1 July 2022

Abstract

The objective of this study is to investigate the adsorption behavior of an electrospun ceria-nanofiber adsorbent in removing pollutants from a simulated solution. Fourier transform infrared spectroscopy and X-ray diffraction were used to characterize this nanofiber composite. Adsorption parameters including contact time, pH, starting arsenic concentration, and adsorbent dose were optimized using batch adsorption studies. After copper was added to nanofiber, maximum removal efficiencies were increased to 96.5% under optimal conditions (1.2 g/L adsorbate dose; 2.0 ppm initial As(III) concentration; and pH of 5.0). Furthermore, the response surface methodology was also successfully applied to the design optimization of the process with central composite design. The Temkin isotherm model ($R^2 = 0.98$) better described the adsorption equilibrium results. The pseudo-second-order kinetic model was followed by adsorption experimental data. Other kinetics theories, such as Elovich, intra-particle, and film diffusion, were also used to develop a better understanding of the adsorption mechanism. The viability of a copper/ceria composite nanofiber in the removal of arsenic demonstrates an emerging candidate in the removal of pollutants from wastewater.

Keywords Adsorption · Electrospun · Nanofiber · Heavy metal · Isothermal kinetics

✉ Dan Bahadur Pal
danbahadur.chem@gmail.com

✉ Vijai Kumar Gupta
vijaifzd@gmail.com; vijai.gupta@sruc.ac.uk

1 Department of Chemical Engineering, Birla Institute of Technology, Mesra, Ranchi 835215, Jharkhand, India

2 Department of Chemical Engineering and Technology, Indian Institute of Technology (BHU), Varanasi 221005, India

3 Department Chemical Engineering and Biochemical, Rajiv Gandhi Institute of Petroleum Technology, Jais, Amethi 229304, Uttar Pradesh, India

4 Department of Public Health, College of Applied Medical Sciences, Khamis Mushait Campus, King Khalid University, Abha, Saudi Arabia

5 Department of Clinical Laboratory Sciences, College of Applied Medical Sciences, King Khalid University, Abha, Saudi Arabia

6 Biorefining and Advanced Materials Research Center, Scotland's Rural College (SRUC), Kings Buildings, West Mains Road, Edinburgh EH9 3JG, UK

7 Center for Safe and Improved Food, Scotland's Rural College (SRUC), Kings Buildings, West Mains Road, Edinburgh EH9 3JG, UK

Introduction

The non-biodegradability of containments such as textile dyes and heavy metals (HMs) and in both, local water supply and industrial wastewater streams, its high toxicity inside the human body via the food chain is a serious environmental and health hazard. These containments can harm the environment and living organisms, as well (Yuan et al. 2021; Pratush et al. 2018). Numerous approaches for removal of these containments from contaminant water have been reported in various studies. Among the technologies utilized were Al/Fe coagulation, chemical oxidation, photocatalysis, ion-exchange, filtration, reverse osmosis, advanced oxidation, and adsorption (Carolin et al. 2017; Sharma et al. 2021; Kumar et al. 2021). These approaches have a number of drawbacks, including a lengthy procedure, standard performance monitoring, the formation of hazardous effluent, high capital and operational costs, and high-tech upkeep. Adsorption is a more cost-effective HMs removal process than existing approaches. Even with its simplicity and high efficiency, adsorption is termed as promising technique and the most widely used technique for containments removal

(Qin et al. 2020). Metal oxides as adsorbents have a wide range of applications for containments removal along with HMs removal. Demonstrations of a variety of metal-based oxides including composites were found to be useful. Zinc oxide, titanium oxide, iron oxide, iron oxide–aluminum oxide, silica–alumina, and further metal oxides with derivatives have been discussed in the literatures (Bhateria and Singh 2019; Wang et al. 2020).

Adsorption through metal oxide requires high surface area. As a response of recent advances in nanoscience and nanotechnology, there seems to be a significant opportunity for the treatment of environmental concerns. Nanosized adsorbents have substantially greater efficiencies and quicker adsorption rates in water treatment than traditional materials, owing to their extremely large surface area (Chai et al. 2021). Large surface area provided more active sites for adsorption. Due to the high surface area requirement, nanoscopic materials have recently got the interest of researchers seeking to develop them as efficient adsorbents for containment (Al-Hetlani et al. 2021). Various studies on nano-based adsorbents, such as nano-beads, nano-composites, and nanofibers, have indeed been performed (He et al. 2021; Fatima et al. 2021). Furthermore, nanofibers have gotten a lot of interest due to their various benefits, including porous structure, higher permeability for gas, and higher specific surface area, all of which should result in a high adsorption efficiency (Foong et al. 2020).

Electrospun nanofibers (ESNF) have received a lot of attention in the perspective of nano-based methods employed in wastewater management. ESNF can be tailored for a certain physicochemical characteristics, morphology, and resilience, as well as post-treated to alter their physiochemical characteristics (Yang et al. 2019). Because the nanomaterial is irreversibly bonded to the surface of the fibers, nailing nanoparticles to the high surface area of ESNF allows for a large exposed surface area and lowers the possibility of material escape into the surroundings. The eroded surface area nanomaterials are vitally useful in refinement since surface area may be associated to utilities such as sorption and oxidization among other things. Researchers showed their interest in ceria, an oxidized derivative of cerium because of its geometrical distinctiveness, ability to arise in a range of sizes with forms and accessible crystal aspects (Olivera et al. 2018). Hu et al. (2008) and Zhong et al. (2007) investigated ceria material with three-dimensional flowerlike morphology and hierarchical structure in the remediation of As(V). This sorbent with interconnected micro- and nanostructures possessed appealing properties such as a large surface area, a unique size and shape, and useful chemical functionalities suitable for heavy HM adsorption. Wang et al. (2017) investigated photocatalytic oxidation of elemental mercury in coal combustion flue gas using electrospun cerium-based TiO_2 nanofibers. Zhang et al. (2016) developed electrospun porous CeO_2 nanofibers with a large surface area for the removal of methyl orange pollutants. It is therefore of intrigue to us to evaluate the ability of using a nanofiber as a metal adsorbing medium. Furthermore, process can be intensified by the addition of an appropriate cocatalyst or supporting material to the surface of an ESNF lets employed as a sorbent in wastewater management (Olteanu et al. 2019).

The goal of this contribution was to introduce ceria nanofiber for adsorption process in wastewater. Electrospinning was used to construct ceria nanofiber. Further, this nanofiber was employed in adoration of arsenic that is known to be highly toxic to all life forms. This element has been classified by the World Health Organization as a group-1 human carcinogenic substance (Nicomel et al. 2016). Further, the adsorption process was intensified by adding copper to create a ceria/copper composite nanofiber. The obtained nanofiber's morphology was studied using Fourier-transform infrared spectroscopy (FTIR), and X-ray diffraction (XRD). Various sets of tests were carried out to explore the effects of pH, interaction time, adsorbent dose, and starting HM ions concentration on the adsorption efficiency of nanofiber composite. In addition, the event was explained using various isotherms and kinetics models. Experiments were also designed using response surface approach.

Experimental

Preparation of nanofibers

Cupric acetate monohydrate (Sigma-Aldrich) precursors and cerium nitrate hexahydrate (Sigma-Aldrich) were used for metal reagents, polyvinyl-pyrrolidone (Sigma-Aldrich) was used for the selecting polymer because it has a very high atomic weight. Acetic acid (SRL) was used as the reducing agent. Ethyl alcohol (Merck) and double distilled water were chosen as the solvent and co-solvent, correspondingly. The 9% (w/v) PVP was added to the glass vial containing ethyl alcohol and was stirred around 3 h. Subsequently, cerium(III) nitrate hexahydrate and (5 mol% Cu) of copper(II) acetate hydrate were added to the vial containing deionized water. The filling of both the vials were mixed collectively and glacial acetic acid was added slowly to the final solution. For synthesizing casting solution for cerium oxide nanofiber, above process was followed but not addition of copper salt. More information on the electrospun process used to prepare ESNF can be found elsewhere (Pal et al. 2017).

Characterization of nanofibers

FTIR spectra of the synthesized nanofibers were analyzed through FTIR spectrometer (Shimadzu, Japan; IR-Prestige 21). XRD studies of the nanofibers were done using

diffracto-meter having Cu-Kα radiation (Rigaku, Smart Lab, Japan). For elemental analysis of samples, we used inductively coupled plasma optical emissions spectrometer (ICP-OES) in spectral range of 160–900 nm.

As(III) pollutant removal adsorption experiments

Batch adsorption studies have been conducted at a room temperature (298 ± 2 K) by the addition of nanofibers in As(III) solutions of 50 mL in various 100-mL glass containers. The solution was then moved with a rotary shaker for 12 h (350 rpm). At the beginning of the experiment the pH was adjusted to 5.0 ± 0.1 by 0.01 M NaOH or CH_3COOH. During each interval, the aqueous reaction solution was decantated and filtered. The concentration of the sample As(III) ions HM using ICP-OES was examined. The q_e (mmol/g) and $\%E$ with Eqs. 1 and 2, respectively, were calculated for As(III) adsorbed capacity and efficiency of adsorption.

$$q_e = \frac{(C_i - C_e)V}{W}, \tag{1}$$

$$\text{Adsorption efficiency } (\%E) = \frac{C_i - C_e}{C_i} \times 100, \tag{2}$$

where C stands for As(III) concentration during experiment, i stands for initial, and e stands for equilibrium. V (in L) stands for volume of solution and W stands for ESNF weight (in g).

Pollutant adsorption equilibrium's modelling and kinetics

The Langmuir, Freundlich, Temkin, and Dubinin–Radushkevitch (D–R) isotherms were employed to simulate the association between the q_e values and pollutant concentrations at equilibrium.

The Langmuir equation (Sharma et al. 2022):

$$q_e = \frac{q_m b_o C_e}{(1 + b_o C_e)}. \tag{3}$$

The Freundlich isotherm (Sharma et al. 2022):

$$q_{max} = K_f C_e^{1/n}. \tag{4}$$

The Temkin model (Ordonez et al. 2020):

$$q_e = \frac{RT}{b_T} \ln\left(K_T C_e\right). \tag{5}$$

The Dubinin–Radushkevich (D–R) model (Ahmad et al. 2020):

$$q_e = q_s e^{(-\beta\varepsilon^2)} \tag{6}$$

ε is the Polanyi potential, which is equal:

$$\varepsilon = RT\left(1 + \frac{1}{C_e}\right). \tag{7}$$

In this equation, R represents the universal gas constant having value of 8.314 J/mol/K). This model uses the evaluate free energy (E) supposed to remove a molecule of adsorbate from its place at the sorption active site and discriminate physical and chemical adsorption. Equation 8 is used to compute E.

$$E\left(\frac{\text{kJ}}{\text{mol}}\right) = \left[\frac{1}{\sqrt{2\beta}}\right]. \tag{8}$$

There are various theories that can be used to predict adsorption kinetics and rate-controlling mechanisms; the most common are the pseudo first (PFO) and second order rate (PSO) theories (Selvakumar and Rangabhashiyam 2019). Furthermore, intra-particle diffusion (IPD) and Elovich (Cai et al. 2019) were used to determine the best adsorption kinetic postulation. The Liquid film diffusion (LFD) in particular, was used to determine whether the sole rate-controlling step was liquid film diffusion or not (Ma et al. 2019). Linearized form of following equations ($y = mx + c$) to all kinetic theories can be plotted.

The PFO theory:

$$q_t = q_e(1 - e^{-k_1 t}) \tag{9}$$

The PSO theory:

$$q_t = \frac{k_2 q_e^2 t}{1 + k_2 q_e t}. \tag{10}$$

The IPD theory:

$$q_t = t^{0.5} \times k_{ipd} + C. \tag{11}$$

The Elovich theory:

$$q_t = \frac{1}{\beta}\log t + \frac{1}{\beta}\log(\alpha\beta). \tag{12}$$

The LFD theory:

$$\ln\left(1 - \frac{q_t}{q_e}\right) = k_{fd} t. \tag{13}$$

Establishment of response surface methodology

The Central Composite Design, which is the standard RSM, was used for the adsorption of pollutant As(III) HM. The

removal of arsenic from wastewater was tested using Ce-based nanofiber and its composite. To optimize the process parameters, a total of 20 experiments (for both nanofiber adsorbents) were designed using Design-Expert 6.0.8. The current study took into account process parameters such as initial pollutant concentration ($Z = 0.8–2.5$ ppm), nanofiber adsorbent dose ($Y = 20–80$ mg), and pH ($X = 3–9$), as well as the percent removal of arsenic. Table 1 shows the range with level of procedure constraints (for both nanofiber adsorbents) considered in the current study.

Results and discussion

Nanofibers characterization

FTIR analysis

The FTIR of prepared pure ceria and composite copper ceria nanofibers are shown in Fig. 1. The broad bands present from 3700 to 2999 cm^{-1} in both nanofibers is because of the stretching vibration of OH group. The important development in the absorption band at 500–1060 cm^{-1} represents structure of ceria nanofiber; these are associated with the emergence of Ce–O bonds (Liu et al. 2008; Pal et al. 2017). The peaks observed at 1625 cm^{-1} and 1620 cm^{-1} are attributed to H–O–H bending. Peaks observed at 1410 and 1360 cm^{-1} were attributed to characteristic peak of CeO_2. Shifting of this peak from 1410 to 1310 cm^{-1} into composite nanofiber attributed to strength in bond between metal oxides. The spectra of nanofibers show several other bands which are more evidently proof in the nanofiber presence of the other functional groups due to solvent (Paschalidou and Theocharis 2019).

XRD analysis

The XRD spectrums of the pure ceria and composite copper ceria nanofibers with varying copper composition are shown in Fig. 2. The spectra's exhibit the distinctive peaks of a fluorite-like cubic phase. There were no peaks seen for the nanofibers at ambient temperature regardless of the composition of cerium salt. This shows that nanofibers obtained at room temperature by the electro-spinning method are amorphous (Cui et al. 2008). After heating, the diffraction peaks for cubic ceria appeared. The more intense reflection of ceria is due to cubic fluorite arrangement with *h k l* value (1 1 1), and monoclinic CuO structure with *h k l* values (2 0 2), at 2θ values of 28.83° and 46.78° respectively. The crystalline size of cerium oxide (15 nm) and composite copper ceria (8–13 nm) were evaluated by Scherer formula. Gautham et al. (2020) also showed ceria with crystalline size 12–16 nm. For ceria–CuO catalyst, it can be shows that copper impregnation influences the ceria lattice constraint slightly. Challenging effects are occupied when doping of fluorite like lattice of ceria with the divalent copper(II) cations is performed. The lesser ionic radii of both copper and copper(II) ions propose that doping lowers the lattice parameter; but, enlarged vacancies (Raitano et al. 2012).

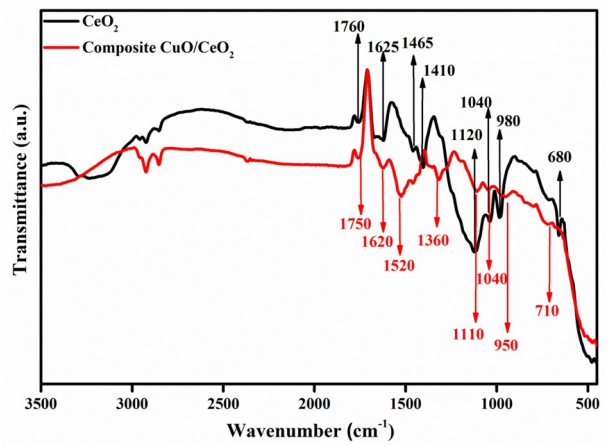

Fig. 1 FTIR spectra of CeO_2 and CuO–CeO_2 nanofibers

Table 1 Actual and coded values of independent variables used for experimental design

Variable	Symbol	Real value of coded levels		
		−1 (low)	0 (medium)	+1 (high)
pH	*X*	3	6.1	9
Adsorbent dose (mg)	*Y*	20	60	80
As(III) concentration (ppm)	*Z*	0.8	1.5	2.5

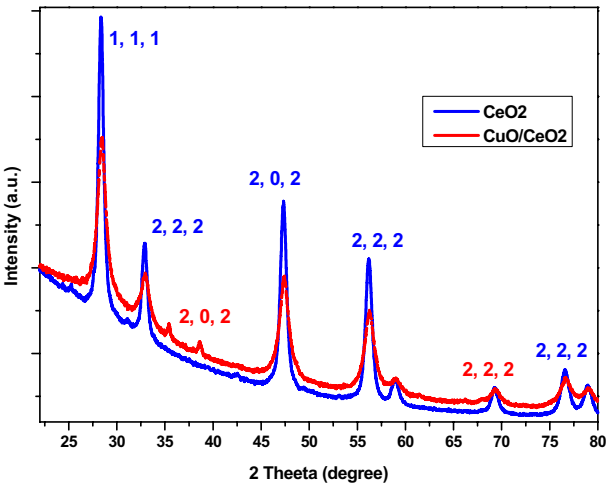

Fig. 2 XRD spectra of ceria and composite CuO/CeO_2 nanofibers

Statistical analysis

Three input factors pH (X), adsorbent dose (Y) and As concentration (Z) and two response variables were used to fitting a quadratic model with the help CCD. The CCD design requires 20 runs based on 3 criteria, the following anticipated responses (Y) for arsenic removal from CeO_2 and CuO/CeO_2 in terms of coded factors were obtained:

$$Y_{As(CeO_2)}(\%) = 91.86 + 2.68X + 1.83Y + 0.45Z - 6.23X^2 - 1.31Y^2 + 0.028Z^2 - 2.13XY + 0.35YZ + 0.28ZX, \quad (14)$$

$$Y_{As(CuO/CeO_2)}(\%) = 93.95 + 2.43X + 1.88Y + 0.49Z - 5.87X^2 - 1.02Y^2 + 0.018Z^2 - 2.29XY + 0.53YZ + 0.31ZX. \quad (15)$$

In this scenario, the ANOVA verifies the model's relevance (the value of probability > F is smaller than 0.05). Each model's p values (probability > F) are less than 0.05, indicating that it is statistically relevant. The ANOVA regression analysis for synthetic wastewater is shown in Table 2. The F values of 30.71 and 39.43 for CeO_2 and CuO/CeO_2, respectively, indicate that the model is substantial. With CeO_2 and CuO/CeO_2, the coefficients of determination (R^2) for As(III) removal were 0.919 and 0.939, respectively. The R^2 value was used to assess the accurateness. Figure 3 depicts a comparison between expected and actual (experimental) response levels. As can be seen from these graphs, there is a great fit between actual and predicted values.

Figure 4, 3D response surface plots are used to determine the effect of time, adsorbent dose and As(III) initial concentration on the responses. 3D plot indicates that there is no much difference on the removal efficiency from the predicted and experimental value from copper oxide ceria composite and ceria. The impacts of factors have a beneficial effect on percentage removal, according to 3D plots. The effectiveness of removal for the two replies is as follows: As(III) removal from copper oxide ceria composite > ceria. All of the 3D charts have distinct peaks. Peaks in 3D plots define the best conditions for maximum response values over the design time, adsorbent dose, and As(III) concentration ranges.

Activity of nanofibers in As(III) removal

Effect of interaction time

The effect of interaction time on the nanofiber's adsorption efficiency was investigated through adding it in As(III) synthetic aqueous solutions at various time duration even as maintaining other parameters constant, such as adsorbent dose (CeO_2 and CuO/CeO_2 nanofiber) and solution pH. The removal of the pollutant As(III) by nanofibers

Table 2 ANOVA analysis for As removal using CeO_2 and CuO/CeO_2

Source	Degree of freedom	Sum of Squares		Mean square		F value		p value Prob > F	
		CeO_2	CuO/CeO_2	CeO_2	CuO/CeO_2	CeO_2	CuO/CeO_2	CeO_2	CuO/CeO_2
Model	9	480.89	436.62	53.43	48.51	17.08	17.08	< 0.0002 (significant)	< 0.0001 (significant)
X	1	74.85	61.36	74.85	61.36	21.60	21.60	0.0018	0.0009
Y	1	28.02	29.71	28.02	29.71	10.46	10.46	0.0277	0.0090
Z	1	2.02	2.42	2.02	2.42	0.85	0.85	0.5056	0.3777
XY	1	36.21	41.77	36.21	41.77	14.70	14.70	0.0151	0.0033
XZ	1	0.65	0.78	0.65	0.78	0.27	0.27	0.7033	0.6114
YZ	1	0.99	2.29	0.99	2.29	0.81	0.81	0.6382	0.3904
X^2	1	302.04	267.65	302.04	267.65	94.21	94.21	< 0.0001	< 0.0001
Y^2	1	11.64	7.04	11.64	7.04	2.48	2.48	0.1280	0.1466
Z^2	1	2.864E−003	1.157E−003	2.864E−003	1.157E−003	4.074E−004	4.074E−004	0.9797	0.9843
Residual	10	42.28	28.41	4.23	2.84	–	–	–	–
Lack of fit	4	42.28	28.41	10.57	7.10	–	–	–	–
Pure error	6	0.000	0.000	0.000	0.000	–	–	–	–

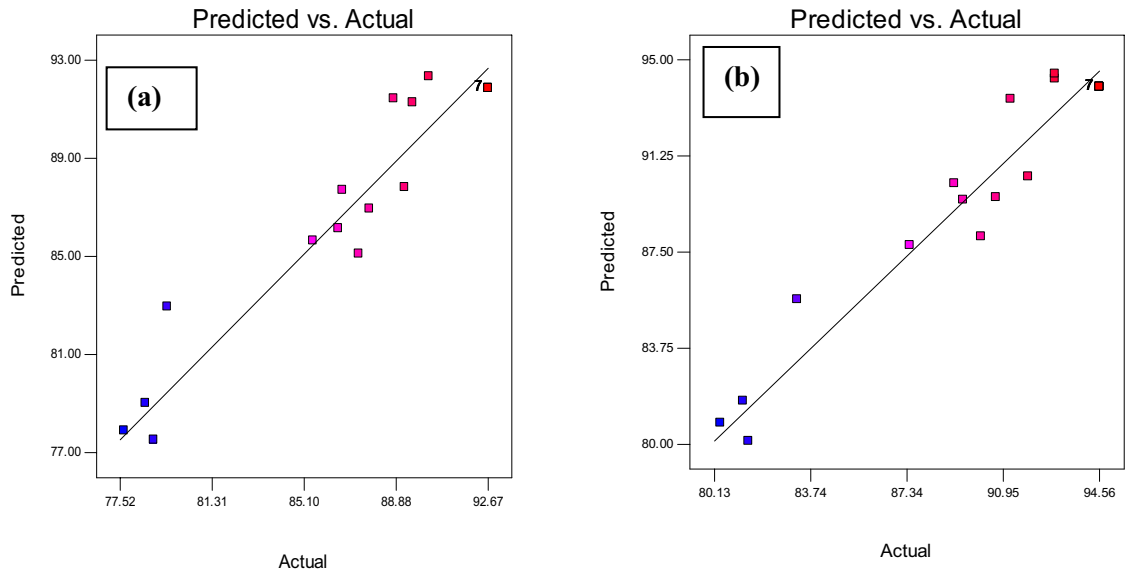

Fig. 3 Plot shows the actual and predicted values of the responses using **a** CeO_2, and **b** CuO/CeO_2

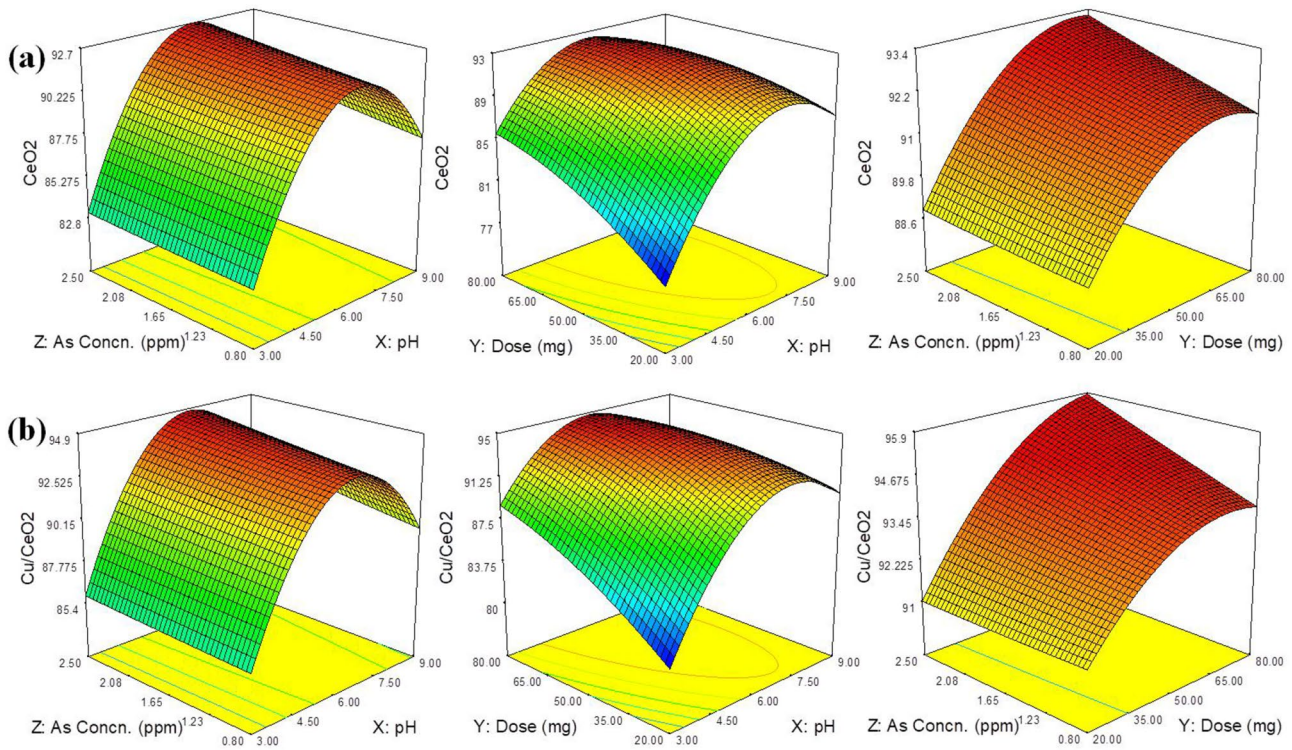

Fig. 4 RSM response curve including effect of different parameters initial concentration of metal ions, nanofiber dose and pH of solution on % As(III) removal using **a** ceria **b** CuO/ceria nanofiber

was observed to be very quick, with an adsorption removal efficiency of 56% quickly after 0.5 h of incubation. This effectiveness progressively increased with increasing contact time, achieving 75% removal at 1 h and saturating (> 89%) around the 1.5-h time interval. This minor change in the adsorption indicates that it has reached an equilibrium state at this point. The availability of active adsorption sites may explain the rapid adsorption of As(III) by CeO_2 (Brandes et al. 2019). The removal efficiency was increased to 93% after the addition of copper. This is due to the synergistic effect of copper in ceria nanofiber.

Effect of pH

The results show that the pH of the solution is important in the removal of As(III) from water by ceria and its composite nanofibers. The results of the experiments showed that ceria nanofibers could capture up to 73.75% of As(III) at pH 3. The electrostatic interaction between ceria nanofiber and As(III) was attributed to this behaviour. As(III) is known to exist in water as a negatively charged species, whereas the charge of ceria nanofiber is pH dependent. Because the adsorbent surface was positively charged, an interaction between ceria nanofiber and As(III) was possible (Babaee et al. 2018). At pH 5, the maximum removal efficiency, 88.76%, was achieved. However, in alkaline medium, removal efficiency decreased. At higher pH, electrostatic repulsion prevailed, resulting in less As(III) removal. Interestingly, after the addition of copper, As(III) adsorption capacities increased in the acidic pH range and decreased significantly in the alkaline pH range. The surface complexation mechanism of As(III) at the metal oxide nanofiber adsorbent surface may be responsible for the increase in removal efficiency (Hu et al. 2017).

Effect of adsorbate (As) concentration on the adsorption

Various concentrations of adsorbate (As) (0.8–2.5 ppm) were employed to evaluate the influence of adsorbate (As) concentration on the adsorption efficiency of the composite nanofibers, while the other parameters, such as adsorbent dose and solution pH remained constant (Fig. 4). For low concentrations of As(III), the ceria nanofiber demonstrated a removal efficiency of 77.2% (0.8 ppm). The removal efficiency increased to 93.5 percent when the initial As(III) concentrations were increased from 0.8 to 2.0 ppm at room temperature. With increasing initial concentration, the adsorption percent decreased slightly. These phenomena can be explained by two factors: (a) from an adsorbate standpoint, increasing adsorbate concentration resulted in a higher concentration ascent. Adsorbates were able to overcome mass transfer resistance and diffuse towards the adsorbent thanks to the high concentration gradient. As a result, as adsorbate concentration increased, so did adsorption quantity. (b) In terms of adsorbent, a higher adsorbate concentration implied a higher chance of adsorbates impacting with adsorption sites. To obtain a saturated condition, the majority of the adsorption sites were occupied as the adsorbate concentration increased (Bulin et al. 2020). As a result of this saturated state, the adsorption percentage decreased. However, the decrease in adsorption percent was slight, indicating that copper/ceria nano-fibres have good on concentration adaptability to As(III).

Effect of dose

Adsorbent dose illustrates adsorbent efficiency, which is an important parameter that directly correlates with adsorption cost. Batch adsorptions on As(III) solution with ceria and copper/ceria composite nanofibers dose 20–80 mg were performed to determine the proper dose as shown in Fig. 4. As percentage and quantity of adsorption rose and declined as the dosage was raised. The adsorption % increased as the number of vacant adsorption sites grew with higher dosage. Two variables may be responsible for the decrease in adsorption quantity as dosage is increased (Shen et al. 2020): (a) under high dosage, the permeation of the adsorbent in solution deteriorated. As a result, some adsorption sites become unavailable, and (b) the absolute amount of As(III) results in a lower adsorbent dosage. The growing tendency of the increase in removal effectiveness with increasing adsorbent dose could be ascribed to the increased surface area available. Adsorbent doses of 0.80 g/L were utilised in subsequent studies.

Adsorption isotherm analysis

Adsorption isotherm procedures are well-known and widely used mathematical methods to determine adsorption capacity in different pollutants removal processes. Adsorption isotherms investigation were carried out for equilibrium data produced at 298 K with As(III) concentrations ranging from 0.4 to 1.6 g/L, an interaction time of 90 min, and a pH of 5.0. Assumptions of the Langmuir isotherm model are that activation energy is the same for all active sites and adsorption may take place due to monolayer coverage. To grasp the feasibility information of adsorption experiments, a dimensionless measure termed a separation factor (R_L) is used. Physical adsorption on surfaces is explained by the Freundlich isotherm model (homogenous and heterogeneous). It is also suitable for monolayer and multilayer adsorption studies. The D–R isotherm theory is used to investigate the type of interaction between the adsorbate and the adsorbent, i.e., nature of adsorption process either physical or chemical.

Therefore, the D–R isotherm theory was used to assess the adsorption data set to establish the type of bonding between arsenic species and ceria and copper/ceria nanofiber. The kind of adsorption mechanism is determined by the mean sorption energy (E) values. The Temkin isotherm postulates crucial information about adsorption heat and binding energy. The heat of adsorption reduces linearly as a consequence of the interaction between the adsorbing element and the adsorbate molecules, according to the Temkin model's predictions.

The graphs for linear mathematical formulations for the Langmuir isotherm, Freundlich isotherm, D–R, and Temkin isotherm models were drawn using their Eqs. 3–6, respectively (Sharma et al. 2022; Ahmad et al. 2020; Ordonez et al. 2020). Table 3 summarizes the models used and the results obtained for their parameters, as well as the correlation coefficients (R^2). The linear Temkin model ($R^2 = 0.98$ and 0.97) describes the adsorption isotherms of the As(III)-ions for all tested samples with the highest correlation coefficient. For As(III) ion metal adsorption on nanofibers, the prevalence of b_T values positive integer implies that the process seems exothermic (Ghosh et al. 2019). As a result, one of the mechanisms involved in metal adsorption on both nanofibers was electrostatic affiliation. The results were consistent with previous pH impact research. Inchaurrondo et al. (2019) also reported the removal of arsenic by employing Fe-doped alumina. This model explains that sorption heat is non-uniformly distributed on the surface of the nanofibers (Khare et al. 2021). Furthermore, the sorption energy, denoted by the Langmuir constant K_L, ranges between 1 and 20 kcal/mol, implying that As(III) adsorption on nanofibers is a combination of both physical and chemical adsorptions. The sorption energy R_L is a separation factor with no dimensions. When R_L values are greater than one, the adsorption process is in an unfavorable state, whereas when R_L values are between 0 and 1, the adsorption process is in a favorable state (Fang et al. 2020). The Langmuir model did not fit the adsorption well, as shown in Fig. 5a and Table 3. However, the separation or equilibrium factor R_L was less than one ($R_L = 0.16$ and 0.097, respectively, for ceria and CuO/ceria nanofiber), indicating that the adsorption was favourable.

Table 3 Equilibrium parameters of arsenic adsorption on CeO_2 and CuO/CeO_2 nanofiber

Isotherm model	Parameters	Nanofiber	
		CeO_2	CuO/CeO_2
Langmuir	q_m (mg/g)	0.92	0.94
	K_L (L/mg)	4.49	8.29
	R_L	0.16	0.097
	R^2	0.94	0.91
Freundlich	K_F (L/mg)	87.1	324.33
	$1/n$	2.05	2.064
	R^2	0.96	0.94
Temkin	b_T (kJ/mol)	1.06	1.00
	K_T (L/mg)	14.08	25.71
	R^2	0.98	0.97
D–R	q_m (mg/g)	20.27	23.86
	β (mol^2/kJ^2)	9.39E−08	6.34E−08
	E_a (kJ/mol)	2.31	2.80
	R^2	0.94	0.93

Kinetic modelling of As(III) adsorption by ceria and CuO/ceria nanofibers

The removal of arsenic from synthetic solution is a function of time, and determining the adsorption rate is critical when designing a process for field applications. The study of the kinetic parameters can provide valuable information about the sorption mechanism. The uptake rate in relation to the contact time governs adsorption efficiency. At specific time intervals ranging from 10 to 120 min, kinetic models were used with an optimized arsenic concentration of 2 mg/L. At an equilibrium pH of 6 at 298 K, 0.8 g/L of adsorbent doses were added to the sample solutions.

The PFO, PSO, Elovich, IFD, and LFD kinetic models were used in this study. The PSO kinetic model assumes that electrons are shared and traded between adsorbate and adsorbent. Intra particle diffusion refers to the movement of adsorbate (solute) ions through the internal pores of adsorbents. During adsorption, the liquid film diffusion model was utilized to determine whether or not an exterior boundary layer formed. The linearized forms of these models are represented by Eqs. 10–13.

The PSO theory was found to be suitable for explaining adsorption due to its high R^2 and excellent agreement of the fitted result with the experiment results. The good fit of adsorption to the PSO model revealed two aspects: (a) adsorption was mostly associated with chemical interactions, and (b) adsorption was primarily associated with physical interactions. (b) Chemical adsorption or surface reaction was the rate-determining step. As demonstrated in Fig. 6 and Table 4, the IPD theory matched the adsorption pretty well, showing that IPD was involved in the adsorption process. Despite this, neither the PFO nor the LFD models

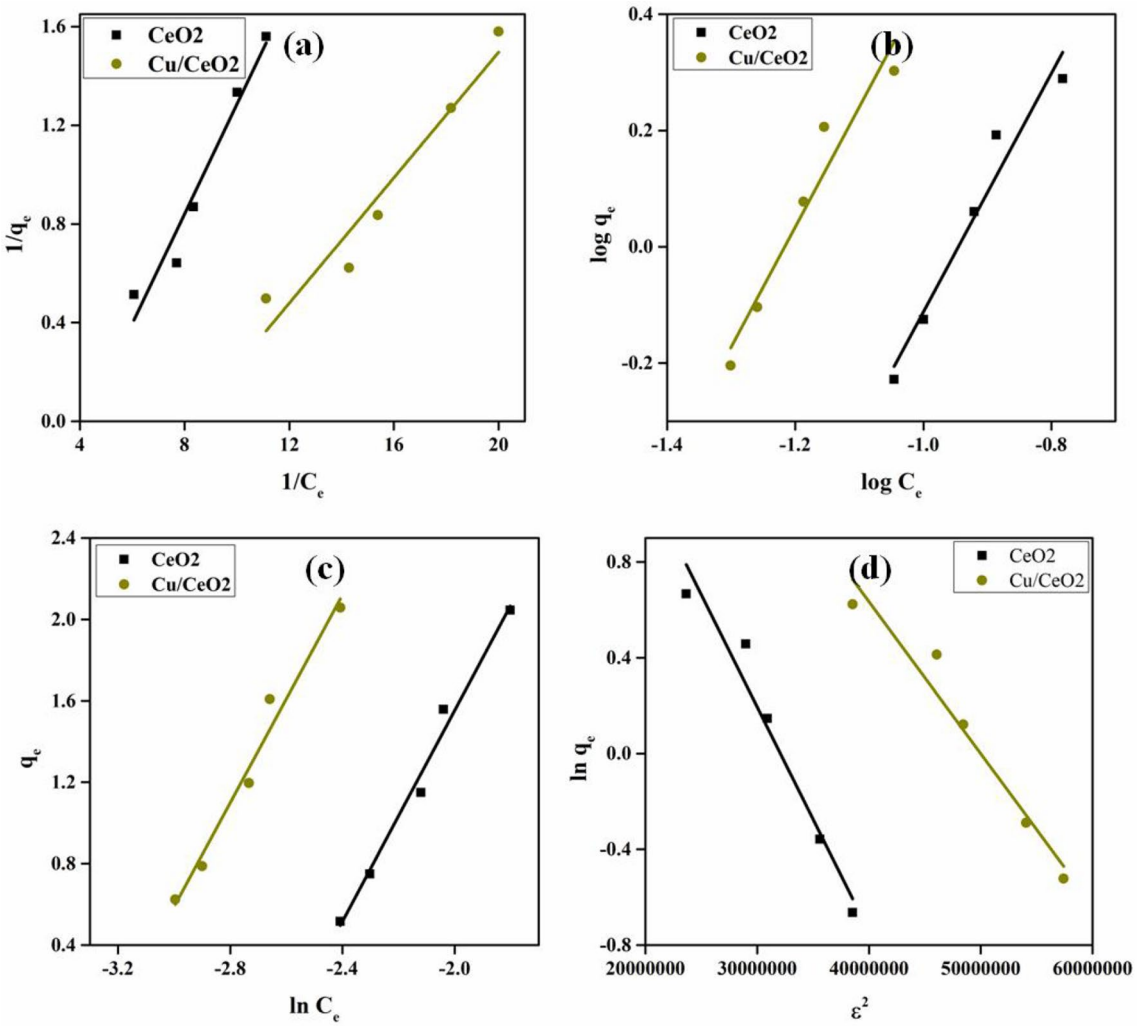

Fig. 5 Isotherm study of As(III) removal equilibrium data on the ceria and CuO/ceria nanofiber **a** Langmuir, **b** Freundlich, **c** Temkin and **d** D–R model

fit the adsorption well, showing that neither the liquid film nor pore diffusion was the rate-determining step. Finally, the entire adsorption process might control using both IPD and chemisorption. Furthermore, the adsorption process is IPD managed when line projections pass through the 0,0 of Cartesian coordinates; otherwise, several processes are engaged in addition to IPD. The graph did not pass through the origin, as shown in Table 4 and Fig. 6d, implying that the adsorption rate of As metal ions on ceria and copper/ceria composite nanofibers may be controlled by the external diffusion process (surface adsorption and liquid film diffusion). Multi-linear plots can be seen in the graph (Fig. 6d), suggesting that the process is regulated by two or more phases (Pholosi et al. 2020). The quick use of the most easily accessible sorbing sites on the sorbent surface can be attributed to the first linear part (phase I) at all concentrations. Phase II might be explained by the slow diffusion of As(III) from the nanofiber surface site into the interior pores. As a result, the first part of As(III) ion sorption by nanofibers may be dictated by the initial intra-particle transport of As(III), which is controlled by surface diffusion, and the second part by pore diffusion.

As(III) removal mechanism

The FTIR and XRD spectra (Figs. 1 and 2) were used to help explain the adsorption phenomenon of As HM pollutant's removal by ceria and CuO/ceria composite

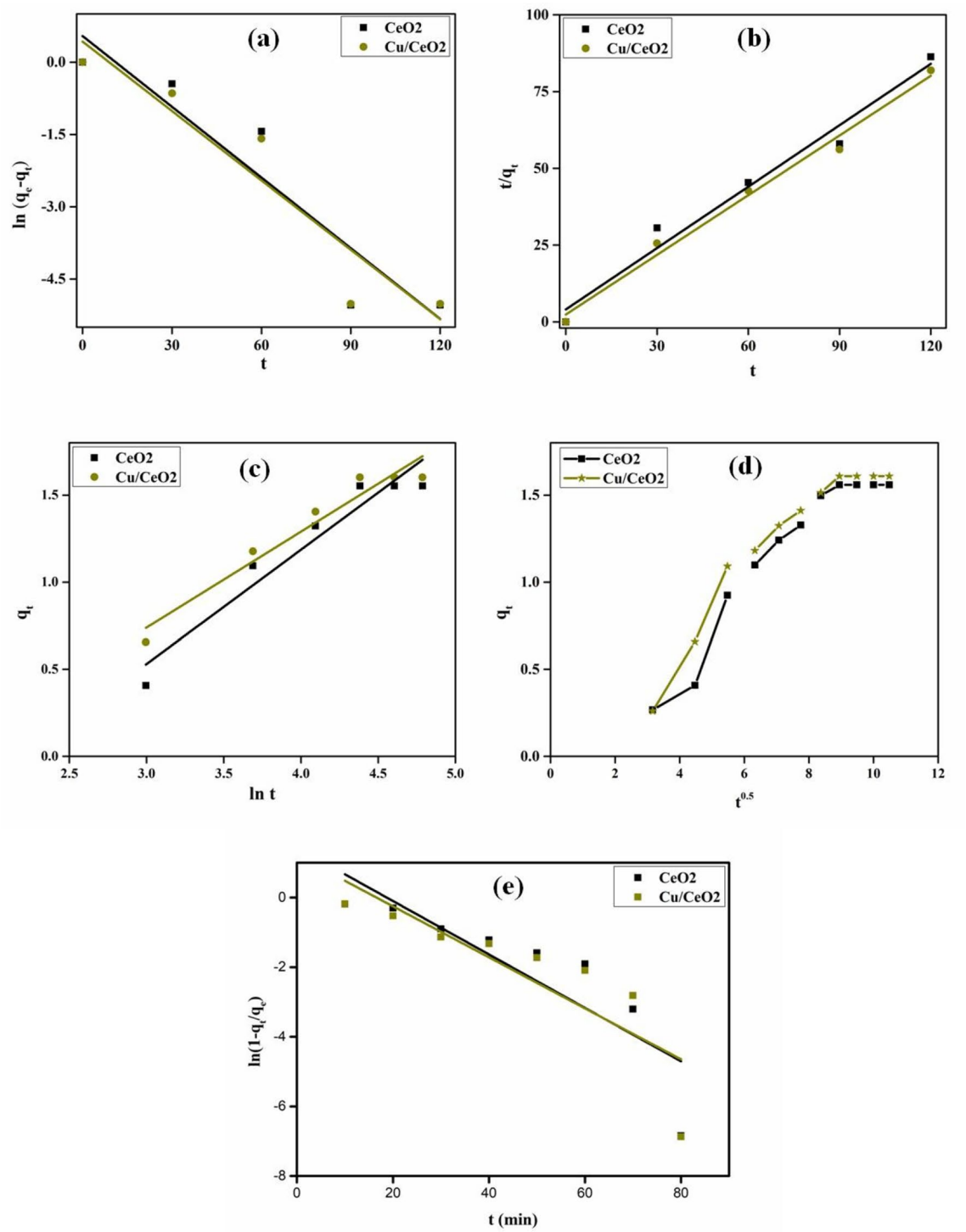

Fig. 6 Kinetic studies employed in As(III) HM ions adsorption on the ceria and CuO/ceria nanofiber **a** PFO equation, **b** PSO equation, **c** Elovich model, **d** IPD and **e** LPD theory

Table 4 Parameters of kinetic theories applied in As(III) adsorption on CeO_2 and CuO/CeO_2 nanofibers

Kinetic model	Parameters	Nano fiber	
		CeO_2	CuO/CeO_2
Pseudo 1st order	$q_{e,cal}$ (mg/g)	3.17	3.69
	k_1 (min^{-1})	0.108	0.113
	R^2	0.885	0.90
Pseudo 2nd order	$q_{e,cal}$ (mg/g)	1.50	1.58
	k_2 (g/mg/min)	0.206	0.210
	R^2	0.985	0.975
Intra particle diffusion			
1st region	$k_{d,1}$ ($mg/g/min^{1/2}$)	0.275	0.356
	C_1	0.67	0.887
	R^2	0.85	0.99
2nd region	$k_{d,2}$ ($mg/g/min^{1/2}$)	0.162	0.162
	C_2	0.082	0.165
	R^2	0.988	0.987
Elovich	α	3.10	1.41
	B	0.309	0.365
	R^2	0.95	0.954
Film diffusion kinetic model	k_{fd} (mg/g/min)	0.67	0.07
	Intercept	1.56	0.76
	R^2	0.74	0.73

nanofibers. According to FTIR analysis, the most common functional groups found on nanofibers are hydroxyl groups. These active sites increased after the addition of Cu. This hypothesis proposed (Hang et al. 2012; Mudzielwana et al. 2020) that metal ions could be coordinated onto active sites of functional groups (Fig. 7). $H_2AsO_3^-$ and $HAsO_3^{2-}$ are negatively charged As(III) ions present in aqueous solution. In the aqueous medium, ceria and CuO/ceria nanofibers are thought to interact with hydroxyl ions and neutral water molecules. The mechanism of arsenic adsorption onto the surface of nanofibers can be seen in Fig. 7. This mechanism could be related to As(III) adsorption. The addition of Cu might provide more active sites for the adsorption of pollutants. As a result, in removing As(III) HM pollutant from simulated wastewater, CuO/ceria composite nanofiber has a higher removal efficiency (96.5%) than bare ceria nanofiber (93.5%).

Surface modification and functionalization all have the potential to improve adsorption capacity. Moreover, membrane preparation using these nanofibers may be a sustainable approach in wastewater treatment (Cui et al. 2020). Some expenses may increase as a result of these changes, necessitating cost optimization.

Conclusion

An electrospinning method was used to develop the highly active CuO/ceria nanofibers. Pollutant As(III) HM ions removal efficiencies were achieved to 92.7% and 96.5%, respectively, with ceria and CuO/ceria composite nanofibers at optimal adsorption conditions of adsorbent dose, starting metal-ion concentration, and 5.0 pH. Equilibrium was achieved within a contact time of 80 min. The maximum adsorption capacities for As(III) adsorption in ceria and CuO/ceria composite nanofibers were 0.91 and 0.93 mg/g, respectively. The adsorption results fitted well with pseudo 2nd order kinetic and Temkin isotherm theories. Response surface methodology with central composite design was successfully applied to optimize the process with F values of 30.71 and 39.43, respectively, for CeO_2 and CuO/CeO_2. Present initial research on ceria nanofibers has demonstrated that nanofibers are effective substances in wastewater treatment. Further, the functionalization, and polymer's cross-linking approaches may be utilized in sustainable technology development.

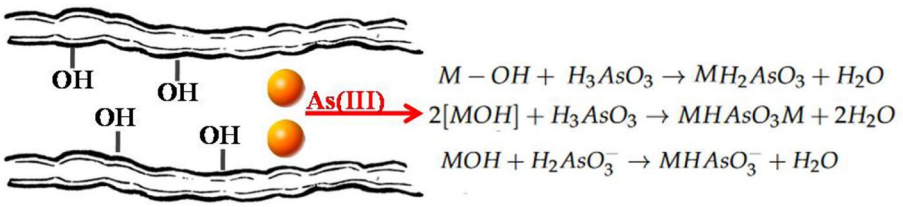

Fig. 7 As(III) removal mechanism

Acknowledgements Authors acknowledge to Department of chemical engineering IIT (BHU) Varanasi and Birla Institute of Technology Ranchi for providing characterization facilities. The authors are grateful to Scientific Research Deanship at King Khalid University, Abha, Saudi Arabia for their financial support through the Large Research Group Project under grant number (RGP.02-87-43).

Author contributions All the co-authors have seen the final manuscript and agreed with the submission to the journal.

Declarations

Conflict of interest There are no conflicts of interest between authors.

Research on human participants and/or animals There is no involvement of human or animal cell in this work.

References

Ahmad M, Usman ARA, Hussain Q, Al-Farraj ASF et al (2020) Fabrication and evaluation of silica embedded and zerovalent iron composited biochars for arsenate removal from water. Environ Pollut 266:115256

Al-Hetlani E, Rajendran N, BabuVelappan A, Amin MO et al (2021) Design and synthesis of a nanopolymer for CO_2 capture and wastewater treatment. Ind Eng Chem Res 60:8664–8676

Babaee Y, Mulligan CN, Rahaman MS (2018) Removal of arsenic(III) and arsenic(V) from aqueous solutions through adsorption by Fe/Cu nanoparticles. J Chem Technol Biotechnol 93:63–71

Bhateria R, Singh R (2019) A review on nanotechnological application of magnetic iron oxides for heavy metal removal. J Water Process Eng 31:100845

Brandes R, Belosinschi D, Brouillette F, Chabot B (2019) A new electrospun chitosan/phosphorylated nanocellulose biosorbent for the removal of cadmium ions from aqueous solutions. J Environ Chem Eng 7:103477

Bulin C, Li B, Zhang Y, Zhang B (2020) Removal performance and mechanism of nano α-Fe_2O_3/graphene oxide on aqueous Cr(VI). J Phys Chem Solids 147:109659

Cai W, Weng X, Chen Z (2019) Highly efficient removal of antibiotic rifampicin from aqueous solution using green synthesis of recyclable nano-Fe_3O_4. Environ Pollut 247:839–846

Carolin CF, Kumar PS, Saravanan A, Joshiba AG et al (2017) Efficient techniques for the removal of toxic heavy metals from aquatic environment: a review. J Environ Chem Eng 5(3):2782–2799

Chai WS, Cheun JY, Kumar PS, Mubashir M et al (2021) A review on conventional and novel materials towards heavy metal adsorption in wastewater treatment application. J Clean Prod 296:126589

Cui Q, Dong X, Wang J, Li M (2008) Direct fabrication of cerium oxide hollow nanofibers by electrospinning. J Rare Earths 26:664–669

Cui J, Li F, Wang Y, Zhang Q, Ma W, Huang C (2020) Electrospun nanofiber membranes for wastewater treatment applications. Sep Purif Technol 250:117116

Fang Y, Wen J, Zhang H, Wang Q, Hu X (2020) Enhancing Cr(VI) reduction and immobilization by magnetic core-shell structured NZVI@MOF derivative hybrids. Environ Pollut 260:114021

Fatima B, Siddiqui SI, Nirala RK, Vikrant K et al (2021) Facile green synthesis of ZnO–$CdWO_4$ nanoparticles and their potential as adsorbents to remove organic dye. Environ Pollut 271:116401

Foong CY, Wirzal MDH, Bustam MA (2020) A review on nanofibers membrane with amino-based ionic liquid for heavy metal removal. J Mol Liq 297:111793

Gautham V, Chinglenthoiba C, John J et al (2020) Enhancement of soot combustion in diesel particulate filters by ceria nanofiber coating. Appl Nanosci 10:2429–2438

Ghosh S, Prabhakar R, Samadder SR (2019) Performance of γ-aluminum oxide nanoparticles for arsenic removal from groundwater. Clean Techn Environ Policy 21:121–138

Hang C, Li Q, Gao S, Shang JK (2012) As(III) and As(V) adsorption by hydrous zirconium oxide nanoparticles synthesized by a hydrothermal process followed with heat treatment. Ind Eng Chem Res 51:353–361

He W, Wang Q, Zhu Y, Wang K, Mao J, Xue X et al (2021) Innovative technology of municipal wastewater treatment for rapid sludge sedimentation and enhancing pollutants removal with nano-material. Bioresour Technol 324:124675

Hu JS, Zhong LS, Song WG, Wan LJ (2008) Synthesis of hierarchically structured metal oxides and their application in heavy metal ion removal. Adv Mater 20:2977–2982

Hu Q, Liu Y, Gu X, Zhao Y (2017) Adsorption behavior and mechanism of different arsenic species on mesoporous $MnFe_2O_4$ magnetic nanoparticles. Chemosphere 181:328–336

Inchaurrondo N, Luca CD, Mori F, Pintar A et al (2019) Synthesis and adsorption behavior of mesoporous alumina and Fe-doped alumina for the removal of dominant arsenic species in contaminated waters. J Environ Chem Eng 7(1):102901

Khare N, Bajpai J, Bajpai AK (2021) Efficient graphene-coated iron oxide (GCIO) nanoadsorbent for removal of lead and arsenic ions. Environ Technol 42(14):2187–2201

Kumar A, Sharma SK, Sharma G, Guo C et al (2021) Silicate glass matrix@Cu_2O/$Cu_2V_2O_7$ p–n heterojunction for enhanced visible light photo-degradation of sulfamethoxazole: high charge separation and interfacial transfer. J Hazard Mater 402:123790

Liu Z, Chen J, Zhou R et al (2008) Influence of ethanol washing in precursor on CuO–CeO_2 catalysts in preferential oxidation of CO in excess hydrogen. Catal Lett 123:102

Ma J, Zhao J, Zhu Z, Li L, Yu F (2019) Effect of microplastic size on the adsorption behavior and mechanism of triclosan on polyvinyl chloride. Environ Pollut 254:113104

Mudzielwana R, Gitari MW, Ndungu P (2020) Enhanced As(III) and As(V) adsorption from aqueous solution by a clay based hybrid sorbent. Front Chem 7:913

Nicomel NR, Leus K, Folens K, Van Der Voort P et al (2016) Technologies for arsenic removal from water: current status and future perspectives. Int J Environ Res Public Health 13(1):62

Olivera S, Chaitra K, Venkatesh K, Muralidhara HB, Inamuddin AAM et al (2018) Cerium dioxide and composites for the removal of toxic metal ions. Environ Chem Lett 16:1233–1246

Olteanu M, Baraitaru A, Panait AM et al (2019) Advanced SiO_2 composite materials for heavy metal removal from wastewater. Water Air Soil Pollut 230:179

Ordonez D, Valencia A, Elhakiem H, Chang N-B, Wanielista MP (2020) Adsorption thermodynamics and kinetics of advanced green environmental media (AGEM) for nutrient removal and recovery in agricultural discharge and stormwater runoff. Environ Pollut 266:115172

Pal DB, Singh P, Mishra PK (2017) Composite ceria nanofiber with different copper loading using electrospinning method. J Alloys Compd 694:10–16

Paschalidou P, Theocharis CR (2019) Surface properties of ceria synthesised using Triton-X based reverse microemulsions. RSC Adv 9(12):7025–7031

Pholosi A, Naidoo EB, Ofomaja AE (2020) Intraparticle diffusion of Cr(VI) through biomass and magnetite coated biomass: a comparative kinetic and diffusion study. S Afr J Chem Eng 32:39–55

Pratush A, Kumar A, Hu Z (2018) Adverse effect of heavy metals (As, Pb, Hg, and Cr) on health and their bioremediation strategies: a review. Int Microbiol 21(3):97–106

Qin H, Hu T, Zhai Y, Lu N, Aliyeva J (2020) The improved methods of heavy metals removal by biosorbents: a review. Environ Pollut 258:113777

Raitano SRJ, Yi N, Zhang L, Chan S-W, Flytzani-Stephanopoulos M (2012) Structure sensitivity of the low-temperature water-gas shift reaction on Cu–CeO_2 catalysts. Catal Today 180:68–80

Selvakumar A, Rangabhashiyam S (2019) Biosorption of rhodamine B onto novel biosorbents from *Kappaphycus alvarezii*, *Gracilaria salicornia* and *Gracilaria edulis*. Environ Pollut 255:113291

Sharma G, Kumar A, Naushad M, Thakur B et al (2021) Adsorptional-photocatalytic removal of fast sulphon black dye by using chitin-cl-poly(itaconic acid-co-acrylamide)/zirconium tungstate nanocomposite hydrogel. J Hazard Mater 416:125714

Sharma G, Kumar A, Ghfar AA, García-Peñas A et al (2022) Fabrication and characterization of xanthan gum-cl-poly(acrylamide-*co*-alginic acid) hydrogel for adsorption of cadmium ions from aqueous medium. Gels 8(1):23

Shen L, Wang J, Li Z, Fan L et al (2020) A high-efficiency Fe_2O_3@ microalgae composite for heavy metal removal from aqueous solution. J Water Process Eng 33:101026

Wang L, Zhao Y, Zhang J (2017) Electrospun cerium-based TiO_2 nanofibers for photocatalytic oxidation of elemental mercury in coal combustion flue gas. Chemosphere 185:690–698

Wang L, Shi C, Wang L, Pan L et al (2020) Rational design, synthesis, adsorption principles and applications of metal oxide adsorbents: a review. Nanoscale 12:4790–4815

Yang D, Li L, Chen B, Shi S, Nie J, Ma G (2019) Functionalized chitosan electrospun nanofiber membranes for heavy-metal removal. Polymer 163:74–85

Yuan X, Xue N, Han Z (2021) A meta-analysis of heavy metals pollution in farmland and urban soils in China over the past 20 years. J Environ Sci 101:217–226

Zhang Y, Shi R, Yang P, Song X, Zhu Y, Ma Q (2016) Fabrication of electronspun porous CeO_2 nanofibers with large surface area for pollutants removal. Ceram Int 42:14028–14035

Zhong LS, Hu JS, Cao AM, Liu Q et al (2007) 3D flowerlike ceria micro/nanocomposite structure and its application for water treatment and CO removal. Chem Mater 19:1648–1655